Effective Algorithm in Steady-State Analysis for Variable-Speed and Constant-Speed Wind Turbine Coupled Three-Phase Self-Excited Induction Generator

Tarek Ahmed*, Katsumi Nishida* and Mutsuo Nakaoka*

Abstract- In this paper, the steady-state operating performance analysis for the three-phase squirrel cage rotor self-excited induction generator (SEIG) driven by a variable-speed prime mover (VSPM) in addition to a constant-speed prime mover (CSPM) is presented on the basis of an effective algorithm based on its frequency-domain equivalent circuit. The operating characteristics of the three-phase SEIG coupled by a VSPM and/or a CSPM are evaluated on line processing under the condition of the electrical passive load parameters variations with simple and efficient computation processing procedure in unregulated voltage control loop scheme. A three-phase SEIG prototype setup with a VSPM as well as a CSPM is implemented for the small-scale clean renewable and alternative energy utilizations. The experimental operating characteristic results are illustrated and give good agreements with the simulation ones.

Keywords: Three-Phase Self-Excited Induction Generator, Variable-Speed and Constant-Speed Wind Turbine, Stand-Alone Power Conditioner, Renewable Energy Sources

1. Introduction

In the stand-alone operation for clean rural alternative energy utilization areas, the three-phase induction generator can operate in the self-excitation power generation mode when an appropriate capacitor bank assembly connected on its stator terminal ports and driven by the renewable energy prime mover as a wind turbine[1], [2]. The three-phase self-excited induction generator (SEIG) determines its own generated terminal voltage and its output frequency, which strongly depend on the capacitance of the fixed excitation capacitor bank, the circuit parameters of the three-phase induction generator, the electrical passive circuit components of the stand-alone load or the independent load and the angular speed of the prime mover as the wind turbine[3-6]. The approximate steady-state circuit analysis in a frequency domain of the three-phase SEIG has been done so far with the following generic assumptions for a few papers presented previously [2-9], that is,

-Iron losses are negligible

-Only fundamental M.M.F. waves are considered

-Resistances and reactances of the three-phase induction generator are constant, except for the magnetizing reactance described graphically by means of the magnetization curve.

-The rate of change in the parameters and variables of the electro-mechanical equivalent circuit is extremely small, so that the per-phase steady-state equivalent circuit in the frequency domain can be used so far.

This paper describes a simple algorithm to evaluate the steady-state operating performance analysis of the three-phase SEIG driven by a variable-speed prime mover (VSPM) as well as a constant-speed prime mover(CSPM) based on the electro-mechanical equivalent circuit representation in the frequency domain basis as promising stand-alone power supplies in rural district.

2. Variable-Speed Prime Mover Characteristics

The mechanical output power P_m of the VSPM is defined as [1-6],

$$P_m = T_m \omega_s \upsilon \tag{1}$$

where υ is the per unit speed of the VSPM (υ=N/N_s) , N and N_s are the rotor speed and the three-phase SEIG synchronous speed in (rpm), respectively. ω_s is the rated synchronous angular speed ($\omega_s = 2\pi N_s/60$). T_m is the mechanical output torque of the VSPM in N.m and represented by,

$$T_m = \tau_o - \upsilon_o \upsilon \tag{2}$$

* Dept. of Electrical and Electronic Engineering, Yamaguchi University, Japan. (tarek@pe-news1.eee.yamaguchi-u.ac.jp)

Received May 7, 2003 ; Accepted June 23, 2003

where τ_o and υ_o respectively are the torque coefficient and the speed coefficient in N.m.

In experiment, a controllable separately-excited dc motor is used with constant armature voltage and a field current control. Fig.1 illustrates the effect of the field current control on the torque speed characteristics and the corresponding torque-speed coefficients τ_o and υ_o which are given by,

$$\tau_o = \frac{K_t \phi_m V_a}{R_a} \quad \text{and} \quad \upsilon_o = \frac{2\pi K_t^2 \phi_m^2}{60 R_a} N_s$$

where K_t is the torque constant , ϕ_m is the field flux in wb per pole of the dc motor, V_a is the armature voltage in volt and R_a is the armature resistance in ohm.

3. Steady-State Analysis of Three-Phase SEIG Driven By Variable-Speed Prime Mover

The nodal admittance approach-based circuit analysis is applied on the approximate frequency domain-based electro-mechanical equivalent circuit of the three-phase SEIG

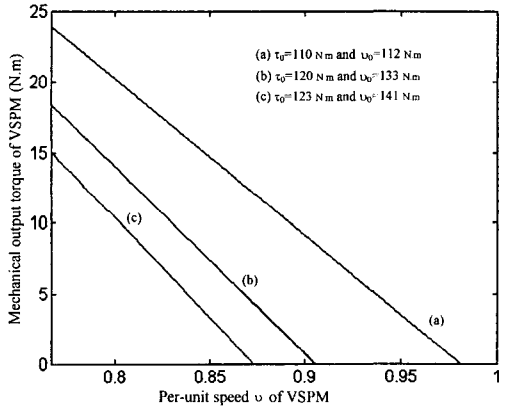

Fig. 1 Mechanical output torque characteristics of VSPM against its per-unit speed

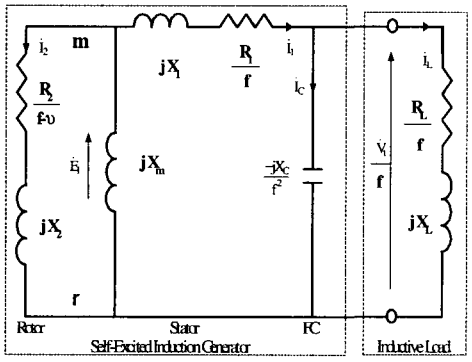

Fig. 2 Per-phase equivalent circuit of three-phase SEIG

in Fig.2 with the per-unit frequency, f (f=F/F_b, F and F_b are the generated output frequency and base frequency of the three-phase SEIG) and the relative rotor speed υ(υ=N/Ns, Ns=1500 rpm when F_b=50 Hz) as state variables.

In Fig.2, R_1, X_1, R_2 and X_2 are the three-phase SEIG parameters referred to its stator winding side, R_L and X_L are the inductive load components in ohm, X_C is the excitation capacitive reactance in ohm (X_C=(1/2πF_bC; F_b=50Hz and C is the excitation capacitance in farad), X_m is the magnetizing reactance in ohm, $\dot{E}_1$, $\dot{V}_t$, $\dot{I}_1$, $\dot{I}_2$, $\dot{I}_L$ and $\dot{I}_C$ are the per-phase air gap voltage in volt, the per-phase generated terminal voltage in volt, the per-phase stator current in ampere, the per-phase rotor current in ampere referred to the stator side, the per-phase load current in ampere and the per-phase excitation current in ampere for the three-phase SEIG, respectively.

The squirrel cage rotor current I_2 referred to the stator winding side of the three-phase SEIG can be defined as,

$$I_2 = \frac{E_1}{R_2\sqrt{\frac{1}{(f-\upsilon)^2} + \left(\frac{X_2}{R_2}\right)^2}} \tag{3}$$

In actual, the term (f-υ) is extremely small from a practical point of view, the term (X_2^2/R_2^2) in (3) could be substantially neglected with respect to $1/(f-\upsilon)^2$. Thus, the above equation of the rotor current I_2 referred to the stator winding circuit side can be expressed by the following simple equation,

$$I_2 = \frac{(f-\upsilon)E_1}{R_2} \tag{4}$$

The mechanical input power P_i(watt) of the three-phase SEIG is estimated by the reference [5]

$$P_i = -3I_2^2 \frac{R_2}{(f-\upsilon)}\left(\frac{\upsilon}{f}\right) \tag{5}$$

By substituting I_2 into (5) and making a mechanical power balance through equating (5) and (1). The per-unit speed υ can be derived as a function of the per-unit frequency f,

$$\upsilon = \frac{(\tau_0 + \frac{3E_1^2}{R_2\omega_s})f}{\upsilon_0 f + \frac{3E_1^2}{R_2\omega_s}} \tag{6}$$

By using the nodal admittance approach on the magnetizing reactance X_m, the following equation can be written as,

$$(\dot{Y}_{mr} + \dot{Y}_m + \dot{Y}_r)\dot{E}_1 = 0 \quad (7)$$

For the successful generated terminal voltage building up of the three-phase SEIG, E_1 does not equal to zero, the relationship of the following nodal admittance yields;

$$\dot{Y}_{mr} + \dot{Y}_m + \dot{Y}_r = 0 \quad (8)$$

where $\dot{Y}_{mr}$, $\dot{Y}_m$ and $\dot{Y}_r$ can be represented by using the equivalent circuit shown in Fig.2 as follow;

$$\dot{Y}_{mr} = \frac{1}{\frac{(\frac{R_L}{f} + jX_L)(\frac{-jX_C}{f^2})}{\frac{R_L}{f} + j(X_L - \frac{X_C}{f^2})} + \frac{R_1}{f} + jX_1} \quad (9)$$

or $\dot{Y}_{mr} = G_{mr} + jB_{mr}$,

where $G_{mr} = \dfrac{D_1 f + D_3 f^3 + D_5 f^5}{D_0 + D_2 f^2 + D_4 f^4 + D_6 f^6}$

and $B_{mr} = \dfrac{(C_0 + C_2 f^2 + C_4 f^4) f^2}{D_0 + D_2 f^2 + D_4 f^4 + D_6 f^6}$

$$\dot{Y}_m = -\frac{j}{X_m} \quad (10)$$

$$\dot{Y}_r = \frac{1}{\left[\frac{R_2}{f - \upsilon} + jX_2\right]}$$

$$\dot{Y}_r = \frac{(-\tau_0 + \upsilon_0 f) f}{(\frac{3E_1^2}{\omega_s} + \upsilon_0 R_2 f) + j(-\tau_0 + \upsilon_0 f) X_2 f} \quad (11)$$

or $\dot{Y}_r = G_r + jB_r$

where $G_r = \dfrac{(A_0 + A_1 f + A_2 f^2) f}{T_0 + T_1 f + T_2 f^2 + T_3 f^3 + T_4 f^4}$

and $B_r = \dfrac{(Q_0 + Q_1 f + Q_2 f^2) f^2}{T_0 + T_1 f + T_2 f^2 + T_3 f^3 + T_4 f^4}$

The constants A_i(i=0~2), D_j(j=0~6), C_k(k=0,2,4), T_l (l=0~4), and Q_h(h=0~2) are estimated in Appendix.

Equating the sum of the imaginary terms in (8) to zero, the magnetizing reactance can be obtained by,

$$X_m = \frac{1}{B_r + B_{mr}} \quad (12)$$

where B_{mr} and B_r are given by (9) and (11), respectively. Equating the sum of the real terms of (8) to zero, the 8th order polynomial equation a function of the per unit frequency f can be written by,

$$Y_8 f^8 + Y_7 f^7 + Y_6 f^6 + Y_5 f^5 + Y_4 f^4 + Y_3 f^3 + Y_2 f^2 + Y_1 f + Y_0 = 0 \quad (13)$$

where the real coefficients from Y_0 to Y_8 can be expressed in Appendix .

To compute the steady-state performance of the three-phase SEIG, the steady-state value of the air-gap voltage E_1 is required. The magnetization curve obtained from the no-load test, which is used to obtain the air-gap voltage E_1 against the magnetizing reactance X_m curve shown in Fig.3, is then represented by the following equation,

$$E_1 = \begin{cases} 207.2 - 3.77X_m & X_m \le 24.2 \\ 541.7 - 17.79X_m & 24.2 \le X_m \le 26.5 \\ 0 & X_m \ge 26.5 \end{cases} \quad (14)$$

By using Newton Raphson method with the initial value of the per-unit frequency $f=\tau_0/\upsilon_0$, the per-unit frequency f can be determined from (13) and can be then substituted into (12) to calculate the magnetizing reactance X_m. The air gap voltage E_1 is estimated from (14).

The following equations are used for describing the three-phase SEIG performances,

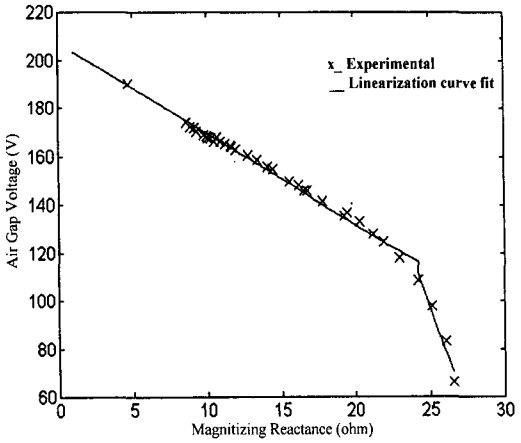

Fig. 3 Air-gap voltage E_1 vs. magnetizing reactance X_m of SEIG

$$V_t = fE_1\sqrt{R_{eq}^2 + X_{eq}^2} \quad (15)$$

where $R_{eq} = X_1 B_{mr} - \dfrac{R_1}{f} G_{mr} + 1$

and $X_{eq} = X_1 G_{mr} + \frac{R_1}{f} B_{mr}$

$$I_L = \frac{V_t}{\sqrt{R_L^2 + f^2 X_L^2}} \tag{16}$$

$$P_L = 3I_L^2 R_L \tag{17}$$

$$Q_L = 3fI_L^2 X_L \tag{18}$$

where V_t, I_L, P_L and Q_L are the per-phase generated terminal voltage of the three-phase SEIG , the per-phase load current, and the total active power and reactive power of the balanced passive load, respectively.

4. Performance Analysis of SEIG with Constant-Speed Prime Mover

The steady-state theoretical algorithm of the three-phase SEIG driven by a VSPM is used to calculate the operating performance evaluations of the CSPM coupled three-phase SEIG. With a constant speed or relative rotor speed υ, the admittances; $\dot{Y}_{mr}$ and $\dot{Y}_m$ have been expressed, respectively by (9) and (10). While $\dot{Y}_r$, a function of the relative rotor speed υ, can be represented from (11) under the conditions of neglecting the coefficient $(3E_1^2/\omega_s)$ and setting to $\upsilon_0=1$ and $\tau_0=\upsilon$ and given by,

$$\dot{Y}_r = \frac{1}{\left[\frac{R_2}{f-\upsilon} + jX_2\right]} \tag{19}$$

or $\dot{Y}_r = \frac{(f-\upsilon)}{R_2 + j(f-\upsilon)X_2}$

The 8th degree polynomial equation represented in the per unit frequency f and defined as (13) is expressed by

$$\begin{aligned} &Y_{8c}f^7 + Y_{7c}f^6 + Y_{6c}f^5 + Y_{5c}f^4 + Y_{4c}f^3 \\ &+ Y_{3c}f^2 + Y_{2c}f + Y_{1c} = 0 \end{aligned} \tag{20}$$

where the real coefficients from Y_{1c} to Y_{8c} are obtained and derived from the real coefficients fromY_0 to Y_8 under the conditions of neglecting the coefficient $(3E_1^2/\omega_s)$ and setting to $\upsilon_0=1$ and $\tau_0=\upsilon$ in the Appendix .The three-phase SEIG performances such as its generated terminal voltage, the load current, and the total active power and reactive power of the balanced inductive load can be calculated under the above conditions by using (15) , (16) , (17) and (18), respectively.

5. Experimental and Simulation Results

5.1 Performance Evaluations of SEIG with Variable-Speed Prime Mover

The steady-state analytical algorithm of the three-phase SEIG driven by a VSPM is based on the per-phase electromechanical equivalent circuit of the three-phase SEIG shown in Fig.2. The nodal admittance approach is applied to determine the characteristics of the three-phase SEIG driven by a variable-speed prime mover VSPM as wind turbine. A feasible prototype of the three-phase SEIG driven by a VSPM represented by a controllable separately-excited dc motor is built and tested actually. The no-load generated terminal voltage vs. the excitation capacitance characteristics, which are selected to be chosen above the minimum value required to build up the terminal voltage of the three-phase SEIG driven by a VSPM is shown in Fig.4. The terminal voltage of the three-phase SEIG driven by a VSPM with a certain torque-speed characteristic (τ_0=120, υ_0=133) increases with the excitation capacitance and also with changing the torque-speed characteristic from (τ_0=120, υ_0=133) to another one (τ_0=110, υ_0=112) as illustrated in Fig.1. Fig.5 indicates the variations of the output frequency of the three-phase SEIG driven by a VSPM against its excitation capacitance at no load with different torque-speed characteristics. The output frequency of the three-phase SEIG decreased with increasing the excitation capacitance from 150 μF to 350 μF at a certain torque-speed coefficients (τ_0=120, υ_0=133 where the VSPM speed decreases in accordance with the torque-speed characteristic of the VSPM shown in Fig.1) and increases linearly with increasing the speed as with another torque-speed coefficients (τ_0=110, υ_0=112). Fig.6 represents the steady-state generated terminal voltage variations of the three-phase SEIG coupled by a VSPM with a certain toque-speed characteristic (τ_0=120, υ_0=133) and its output power when it is excited by three different capacitances of the excitation capacitor bank (C=194μF, 244μF, and 294μF per-phase) and supplying to a balanced three-phase resistive load. Fig.7 depicts the generated terminal voltage variations against the VSPM speed according its specified torque-speed characteristic when the three-phase SEIG loaded by a balanced resistive load. Fig.6 and Fig.7 indicate that the generated terminal voltage of the three-phase SEIG driven by a VSPM decreases as increasing its output power, which also decreases the VSPM speed. The VSPM speed decreases in accordance with the torque-speed char-

acteristic of the VSPM from the no load N=1360 rpm to the full load N=1220 rpm. For an inductive load condition with 0.8 lagging power factor, a certain torque-speed coefficients (τ_0=120, υ_0=133) and various capacitances (C=194 μF, 244 μF, and 294 μF per phase) of the excitation capacitor bank, Fig.8 illustrates the three-phase SEIG terminal voltage variations with the output power calculated from the digital simulation and experimental results. In Fig.9, the terminal voltage vs. the VSPM speed with a certain toque-speed characteristic (τ_0=120, υ_0=133) is represented due to the inductive load variations. Fig.8 and Fig.9 indicate that the generated terminal voltage tends to fall steeply with the balanced three-phase inductive load as compared with the resistive load. The maximum output power can be found to be less than that to be supplied to a resistive load and the prime mover speed decreases in accordance with the torque-speed characteristic of the VSPM from the no load rotor speed N=1360 rpm to the full load rotor speed N=1260 rpm. With inductive loads, the terminal excitation capacitors must provide the reactive load power to the inductive load in addition to reactive load power to the three-phase SEIG. Therefore, an additional shunt capacitance would be required for improved voltage regulation.

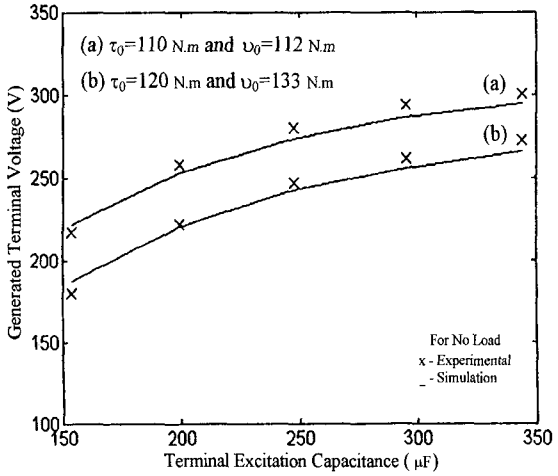

Fig. 4 No load terminal voltage variations of SEIG driven by VSPM vs. excitation capacitance

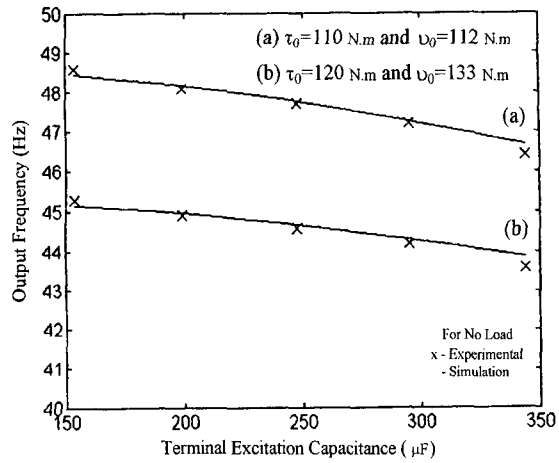

Fig. 5 Output frequency variations of SEIG driven by VSPM vs. excitation capacitance

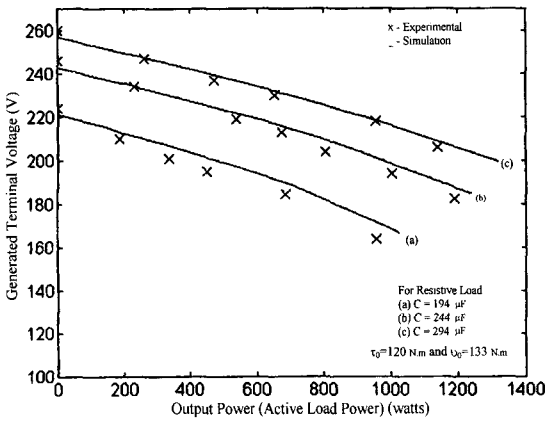

Fig. 6 Terminal voltage variations of SEIG driven by VSPM vs. the resistive load power

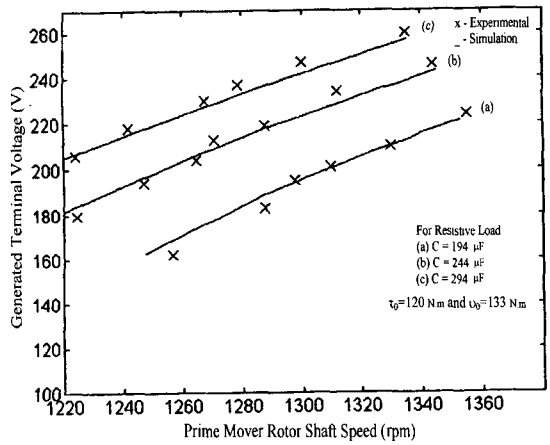

Fig. 7 Terminal voltage of SEIG driven by VSPM against its rotor speed due to the resistive load variations

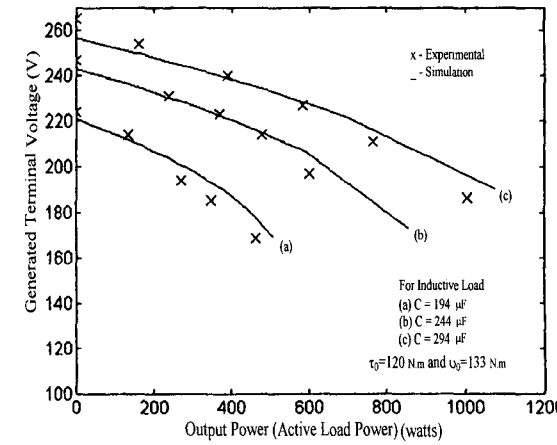

Fig. 8 Terminal voltage variations of SEIG driven by VSPM against the inductive load power

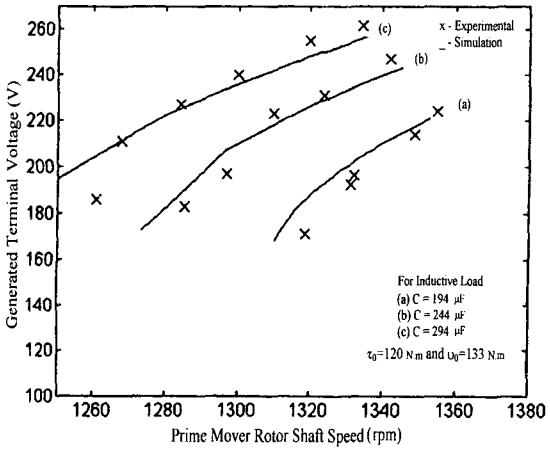

Fig. 9 Terminal voltage variations of SEIG driven by VSPM against its rotor speed due to the inductive load variations

5.2 Performance Evaluations of SEIG with Constant-Speed Prime Mover

For the three-phase SEIG driven by a CSPM with different constant speeds; N=1400 rpm, N=1300 rpm and N=1250 rpm, the no-load generated terminal voltage vs. the excitation capacitance characteristics which are selected to be chosen above the minimum value required to build up the three-phase SEIG terminal voltage is shown in Fig.10. The terminal voltage of the three-phase SEIG increases with the capacitances of the excitation capacitor bank at a constant speed and with increasing the CSPM speed. Fig.11 indicates the variations of the output frequency of the three-phase SEIG against its excitation capacitance with different constant speeds; N=1400 rpm, N=1300 rpm and N=1250 rpm. The output frequency of the three-phase SEIG driven by a CSPM slightly changes with increasing the excitation capacitance from 150 μF to 350 μF and increases linearly with increasing the CSPM speed. Fig.12 gives the load characteristics of the three-phase SEIG terminal voltage with the output power for a fixed capacitance of the excitation capacitor bank at a constant speed N=1300 rpm when supplying a resistive load. The terminal voltage variation is shown in the same figure for three values of excitation capacitances (C=244μF, 294μF and 344μF per-phase). The terminal voltage drops with increasing the load power and increases with increasing the capacitance of the excitation capacitor bank. Also, at the lower capacitance, the maximum output power extracted from the three-phase SEIG is lower than for the higher capacitance. Fig.13 depicts the variation of the terminal voltage of the three-phase SEIG with its output power for an inductive load with 0.8 lagging power factor under the conditions of various capacitances of the excitation capacitor bank and a constant speed N=1300 rpm. The terminal voltage of the three-phase SEIG drops with increasing the inductive load and the maximum output power

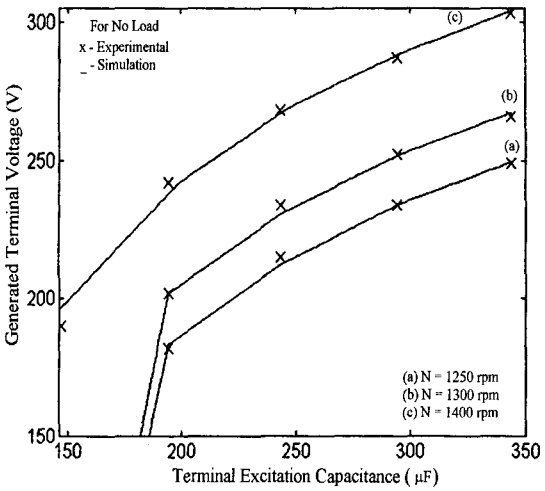

Fig. 10 No load terminal voltage of SEIG driven by CSPM vs. excitation capacitance

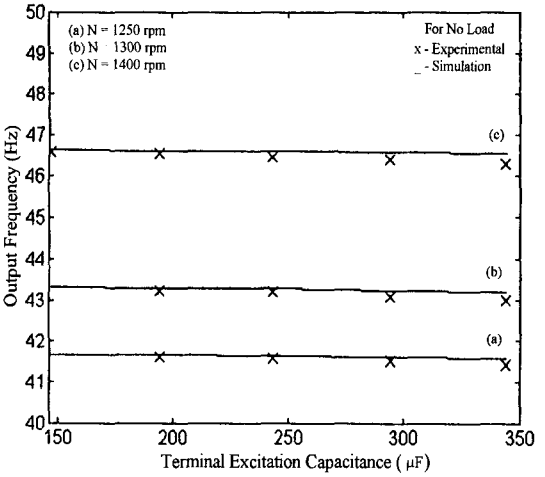

Fig. 11 Output frequency of SEIG driven by CSPM vs. excitation capacitance

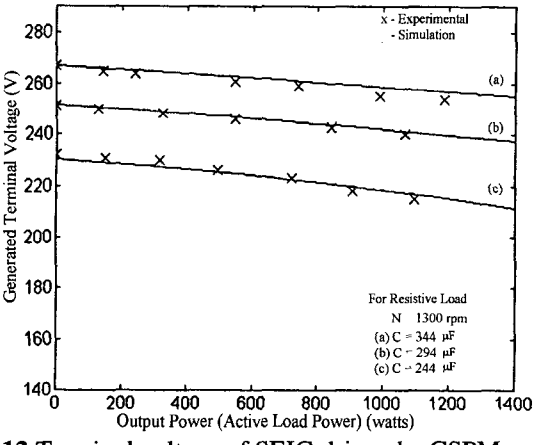

Fig. 12 Terminal voltage of SEIG driven by CSPM vs. the resistive load power

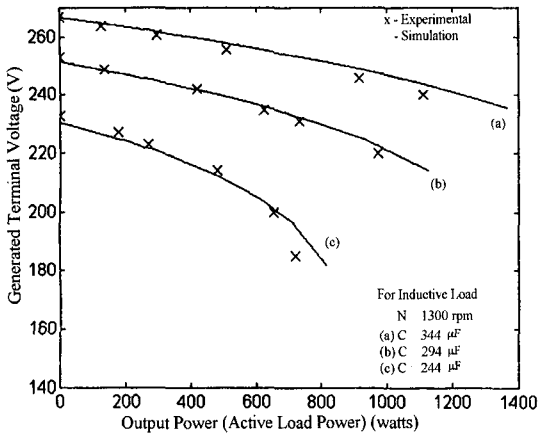

Fig. 13 Terminal voltage of SEIG driven by CSPM against the inductive load power

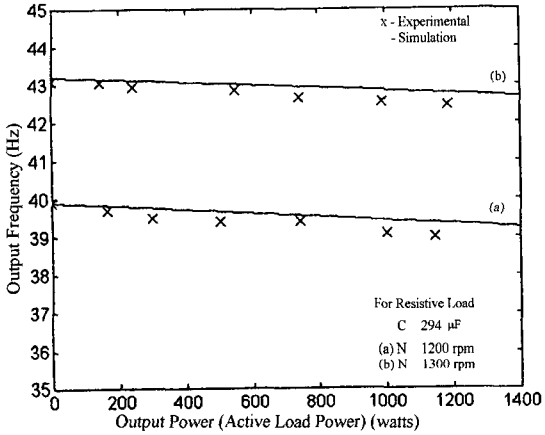

Fig. 14 Output frequency of SEIG driven by CSPM against the resistive load power

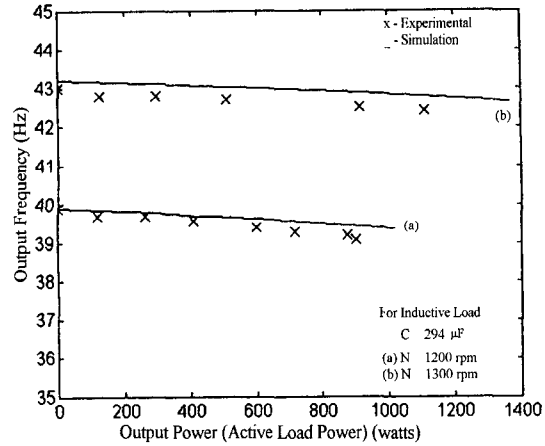

Fig. 15 Output frequency of SEIG driven by CSPM against the inductive load power

extracted from the three-phase SEIG increases with the CSPM than that with the VSPM. Fig.14 and Fig.15 show the output frequency variations of the three-phase SEIG against its output power for both a resistive and an inductive loads, respectively with a fixed excitation capacitance C=294μF and different values of constant speeds. The output frequency of the three-phase SEIG drops from the no load to the full load which means that the output frequency of the three-phase SEIG changes with the load power variations but with small variation ranges. The frequency variations increase with the inductive load.

6. Conclusions

This paper has introduced an effective theoretical algorithm for the steady-state frequency domain circuit analysis and operating performance evaluations based on the electro-mechanical equivalent circuit of the three-phase SEIG driven by a VSPM in addition to a CSPM. A squirrel cage three-phase SEIG prototype setup was established for the low cost wind turbine type rotating power conditioner in the rural alternative energy effective utilization areas from an earth environmental protection point of view. The feasible experimental results in the steady-state operating performances of the three-phase SEIG had pretty good agreements with those obtained from the digital simulation ones.

References

[1] M.Konstenko and L.Piotravsky, "Electrical Machines", Mir Publishers, Moscow, 1969.

[2] T.F.Chan, "Analysis of Self-Excited Induction Generator Using an Iterative Method", IEEE Trans. on Energy Conversion, Vol.EC-10, No.3 pp.502-507, September, 1985.

[3] S.P.Singh , M.P.Jain and Bhim Singh, "A New Technique for Analysis of Self-Excited Induction Generator", Journal of Electric Machine and Power Systems, Vol.23, pp.647-656, 1995.

[4] A. Koyanagi "Maximum Power Point Tracking of Wind Turbine Generator Using a Flywheel", Proceedings of the 2001 IEE-Japan Industry Application society Conference, Vol.1, pp395-398, 2001.

[5] S.Rajakarvna and R.Bonert, "A Technique for The Steady State Analysis of Self-Excited Induction Generator with Variable Speed", IEEE Trans. on Energy Conversion, Vol.10, No.1 pp.10-16, March, 1995.

[6] W. Koczara, "Variable Speed Three-Phase Power Generation Set", Proceedings of EPE, September, 2001.

[7] A. Koyanagi "Maximum Power Point Tracking of Wind Turbine Generator Using a Flywheel", Proceedings of the 2001 Japan Industry Application society Conference, Vol.1, pp395-398, 2001.

[8] Tarek Ahmed, Osamu Noro, Koji Sato, Eiji Hiraki and Mutsuo Nakaoka "Single-Phase Self-Excited Induc-

tion Generator with Static VAR Compensator Voltage Regulation for Simple and Low Cost Stand-Alone Renewable Energy Utilizations Part I: Analytical Study" KIEE International Transactions on Power Engineering, Vol.3-A, No.1, pp.17-26, 2003.

[9] Tarek Ahmed, Osamu Noro, Koji Sato, Eiji Hiraki and Mutsuo Nakaoka "Single-Phase Self-Excited Induction Generator with Static VAR Compensator Voltage Regulation for Simple and Low Cost Stand-Alone Renewable Energy Utilizations Part II: Simulation and Experimental Results" KIEE International Transactions on Power Engineering, Vol.3-A, No.1, pp.27-34, 2003.

Appendix

$A_0=G_0G_2$,
$A_1=G_1G_2+G_0G_3$,
$A_2=G_1G_3$,
$D_0=Z_0^2$,
$D_2=Z_1^2+2Z_0Z_2$,
$D_4=Z_2^2+2Z_3Z_1$,
$D_6=Z_3^2$,
$D_1=-X_CZ_0$,
$D_3=R_LZ_1+X_LZ_0-Z_2X_C$,
$D_5=R_LZ_3+X_LZ_2$,
$C_0=-Z_1X_C-R_LZ_0$,
$C_2=Z_1X_L-Z_3X_C-Z_2R_L$,
$C_4=Z_3X_L$,
$T_0=G_0^2$,
$T_1=2G_0G_1$,
$T_2=G_1^2+G_2^2X_2^2$,
$T_3=2G_2G_3X_2^2$,
$T_4=G_3^2X_2^2$,
$Q_0=-G_2^2X_2$,
$Q_1=-2G_2G_3X_2$,
$Q_2=-G_3^2X_2$,

$Z_0=-R_1X_C-X_CR_L$,
$Z_1=X_CX_L+X_1X_C+R_1R_L$,
$Z_2=R_1X_L+X_1R_L$, $Z_3=-X_1X_L$,

$Y_0=T_0D_1+A_0D_0$,
$Y_1=T_1D_1+A_1D_0$,
$Y_2=T_2D_1+T_0D_3+A_0D_2+A_2D_0$, $Y_3=T_3D_1+T_1D_3+A_1D_2$,
$Y_4=T_4D_1+T_2D_3+T_0D_5+A_0D_4+A_2D_2$ $Y_5=T_3D_3+T_1D_5+A_1D_4$,
$Y_6=T_4D_3+T_2D_5+A_0D_6+A_2D_4$,
$Y_7=T_3D_5+A_1D_6$,
$Y_8=T_4D_5+A_2D_6$

Where $G_0=3E_1^2/\omega_s$, $G_1=\upsilon_0R_2$, $G_2=-\tau_0$ and $G_3=\upsilon_0$,
$R_1=0.52$ ohm, $X_1=1.01$ ohm, $R_2=0.52$ ohm,
$X_2=1.01$ ohm,
$\tau_0=120$, $\upsilon_0=133$, $N_s=1500$ rpm, $\omega_s=2\pi N_s/60.0$,

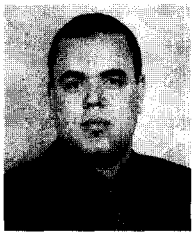

Tarek Ahmed
He received his M Sc.-Eng from the Electrical Engineering Department, Assiut University, Egypt in 1998. He is currently a Ph. D. candidate student in the Graduate School of Science and Engineering, the Power Electronic System and Control Engineering Laboratory at Yamaguchi University, Yamaguchi, Japan. His research interests are in the area of the new applications for the power electronic circuits and systems with the renewable energy and power systems and semiconductor power conditioners. Mr. Ahmed is a student-member of the IEEE and the Japan Society of the Power Electronics.
Tel: +81-836-85-9472, Fax: +81-836-85-9401

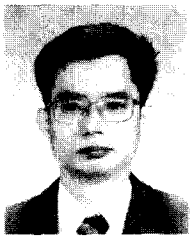

Katsumi Nishida
He received the B.S., and M.S. degrees in electrical engineering from the Tokyo Institute of Technology, Tokyo, in 1976, 1978, respectively. He received the Ph.D. degree from Yamaguchi University, Yamaguchi, in 2002. He is engaged in research on power factor correction of PWM converter and current control of three-phase active power filter with dead-beat technique and adaptive signal processing technique. Dr. Nishida is a member of the Institute of Electrical Engineers of Japan.

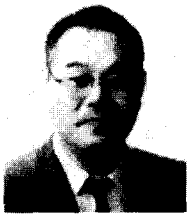

Mutsuo Nakaoka
He received his Dr-Eng. degree in Electrical Engineering from Osaka University, Osaka, Japan in 1981. He joined the Electrical and Electronics Engineering Department of Kobe University, Kobe, Japan in 1981. Since 1995, he has been a professor of the Electrical and Electronics Engineering Department, the Graduate School of Science and Engineering, Yamaguchi University, Yamaguchi, Japan. His research interests include application developments of power electronics circuit and systems. He received the 2001 premium paper award from IEE-UK and so on. Dr. Nakaoka is a member of the Institute of Electronics, Information and Communication Engineers of Japan, Institute of Illumination Engineering of Japan, European Power Electronics Association, the Japan Society of the Solar Energy, IEE-Korea and IEEE.